Composites: Part A 174 (2023) 107712

Contents lists available at ScienceDirect

Composites Part A

journal homepage: www.elsevier.com/locate/compositesa

# Towards a virtual test framework to predict residual compressive strength after lightning strikes

S.L.J. Millen [a,*], X. Xu [b], J. Lee [d], S. Mukhopadhyay [e], M.R. Wisnom [c], A. Murphy [a]

[a] School of Mechanical and Aerospace Engineering, Queen's University Belfast, Ashby Building, Belfast BT9 5AH, Northern Ireland, UK
[b] Centre for Aeronautics, School of Aerospace, Transport and Manufacturing, College Road, Cranfield MK43 0AL, UK
[c] Bristol Composites Institute, University Walk, Bristol BS8 1TR, UK
[d] Department of Mechanical and Aerospace Engineering, Utah State University, Logan, UT 84322-4130, USA
[e] Department of Mechanical Engineering, Indian Institute of Technology, Kanpur 208 016, India

ARTICLE INFO

*Keywords:*
B. Delamination
B. Thermomechanical
C. Finite Element Analysis (FEA)
Compression after Lightning Strikes (CAL)

ABSTRACT

A novel integrated modelling framework is proposed as a set of coupled virtual tests to predict the residual compressive strength of carbon/epoxy composites after a lightning strike. Sequentially-coupled thermal-electric and thermo-mechanical models were combined with Compression After Lightning Strike (CAL) analyses, considering both thermal and mechanical lightning strike damage. The predicted lightning damage was validated using experimental images and X-ray Computed Tomography. Delamination and ply degradation information were mapped to a compression model, with a maximum stress criterion, using python scripts. Experimental data, in which artificial lightning strike and compression testing were performed, was used to assess the predictive capabilities of the framework, considering three lightning strike peak current amplitudes (25, 50, and 75 kA). The framework herein achieved a residual strength prediction within 6% of the experimental values for all peak currents. The relationship between individual lightning damage morphologies (thermal, mechanical and delamination damage) and CAL strength has been numerically established.

## 1. Introduction

Composite materials are more susceptible to lightning strike damage than legacy metal airframes. Therefore, research into lightning strike damage and protection systems, has been receiving increasing attention. Experimental and numerical research has been conducted on lightning strikes, with primary focus on high peak current Waveforms A or D [1–9].

### 1.1. Literature review

Lightning strike simulations have primarily focussed on the thermal-electric effect in the specimen due to resistive heating [5,6,10,11]. For example, Shah and Lee [10] presented a novel stochastic modelling framework predicting lightning thermal damage considering random distributions of electrical conductivity and voids. Other works have focussed on dynamic mechanical pressure loading [12–14], (e.g. Li et al. [14] studied the shock wave pressure induced by impulse currents on carbon fibre reinforced polymers (CFRP) laminates), thermal expansion [15–17], (e.g. Foster et al. [17] quantified the magnitude of internal specimen mechanical loading resulting from electrical load induced thermal expansion), or representing electrical, thermal and mechanical effects [5,16,18] (e.g. Millen et al. [18] used predictions from a lightning plasma model and represented a pressure load, current load, and the resulting thermal and mechanical damage mechanisms).

Simulations have been used to a limited degree to predict residual strength after lightning strikes. Wang et al. [19,20] performed numerical and experimental investigations to predict the residual strength of composite specimens exposed to lightning strikes. In ref. [20], lightning thermal damage in the composite specimen was calculated using a thermal-electric analysis before transferring a damaged state to a structural analysis, and residual tensile strength was predicted using the Hashin failure criteria. Mechanical properties of the remaining elements were degraded with respect to their temperature. However, the modelling approach developed in the work solely considered thermal damage resulting from Joule heating, and thus dynamic mechanical pressure loading and thermal-expansion effects were ignored. In ref. [19], post-lightning strike residual strength under axial compression loading was

* Corresponding author.
*E-mail address:* scott.millen@qub.ac.uk (S.L.J. Millen).

https://doi.org/10.1016/j.compositesa.2023.107712
Received 23 March 2023; Received in revised form 17 July 2023; Accepted 30 July 2023
Available online 31 July 2023

considered, and simulation and experimental data were compared. The authors found that compressive failure load decreased with increased applied action integral (defined as the time integral of the current squared), and therefore increased specimen damage. As before, the lightning strike modelling was limited to thermal-electric loading, i.e. without representation of the lightning mechanical loading. In addition, no delamination behaviour was explicitly modelled through cohesive interactions or other means. Therefore, the detailed failure mechanisms between the pristine specimens and the lightning damaged specimens could not be fully compared.

Most recently, Harrell et al. [5,21] proposed a modelling framework to predict dielectric breakdown, using a quarter model and a radially expanding lightning arc. The authors validated their model [5] with conventional damage models [16]. However, this comparison did not make use of the actual referenced conventional damage model, rather, the authors modified their own model and compared prediction variation. Harrell et al. [21] used sequential simulations, in which lightning damage was transferred using a point cloud transformation approach, to a structural scale model which was used to predict the structural response of the damaged CFRP laminate. The simulation chain only considered dielectric breakdown and Joule heating as the primary contributors to lightning damage.

Literature is replete with studies on the compression after impact (CAI) strength of composite specimens e.g. [22–26]. In contrast, only three of the previously discussed papers on modelling lightning damage considered in-plane compressive residual strength [19,27,28]. From the literature clear methods have been developed to illuminate the damage considering the key lightning physics (plasma, thermal-electric, pressure/thermal-expansion) [16,18]. In addition, methods to represent lightning strike damage within post-strike mechanical testing has been demonstrated [20,21]. However, preceding work has clearly not represented all forms of loading and damage in a complete simulation chain. Preceding works have therefore neglected some of the key lightning physics in the prediction of residual strength.

Experimental works have studied the residual strength of composite specimens subjected to lightning strikes with the use of tensile, compressive, or flexural testing [8,19,20,27,29–34]. Recently, attempts have been made to adapt the standard CAI test method for the assessment of post-strike compressive strength [19,35]. In preceding work by the authors, Xu et al. [35], a systematic experimental study was completed to find an optimal Compression after Lightning Strike (CAL) test method. CAL tests were completed on composite specimens after lightning strikes of modified Waveform D between 25 and 100 kA peak amplitudes. For peak currents of 50 and 75 kA, compression failure did not occur at the lightning damage area (central failure), rather at the test boundary conditions (edge failure). The authors identified an unsupported gap in the CAI jig as the determining factor in central versus edge failure. The unsupported gap is defined as the region of material on each side of the test specimen which is not gripped by the test machine. Results showed that CAL strength at 25 kA reduced by 28% from the pristine compressive strength of the specimen. Results were in agreement with the majority of works that increasing peak current reduces the composite residual strength [20,28,35,36].

### 1.2. Summary

Lightning strike experimental and simulation research has produced limited study of the residual strength following lightning strikes. A near universal observation has been made that increasing peak current is directly correlated with a reduction in residual strength. However, the details of composite specimen failure, experimental evidence of different damage modes (thermal, mechanical, and delamination damage) and the link between each damage mode and residual strength have not received as much attention. For example, none of the previously published experimental works studying post-lightning compressive residual strength have described the detailed failure mechanisms associated with the lightning damage and how these influence the failure mechanics under compressive loading.

A small number of simulation studies have attempted to model the residual strength tests, but again these are not focused on representing failure considering all potential forms of damage, that would enable the detailed and accurate prediction of both interlaminar and intralaminar failure initiation and propagation. Therefore, there is incomplete knowledge on how lightning (i.e., high impulse current waveform loading) influences the extent and shape of damage in composite specimens, and how this damaged state is correlated to the mechanisms of failure which are witnessed in the overall reduction in residual strength.

Therefore, the novelty of this work is to make use of experimental observations [35], and a mature simulation chain, which has been verified previously [11,16] to create a virtual test framework to predict residual compressive strength after lightning strikes. The requirements of this virtual test framework are to accurately predict the thermal damage from Joule heating, inter-ply delamination and mechanical damage, resulting from the combination of mechanical and thermal strains and the resulting CAL strength for a given combination of peak current waveform, layup, material and boundary conditions. Once validated this framework will correlate both lightning damage and residual strength with a peak current amplitude and illuminate the likely contributions of thermal, mechanical and delamination damage to residual strength.

## 2. Methodology

### 2.1. Combination of models

An appropriate set of simulation methods was assembled from existing open literature to study the residual CAL strength and associated damage mechanisms. Fig. 1 shows an analysis workflow assembled for the work herein, extending the workflow outlined in ref. [11], with the consideration of lightning test Waveform D and the addition of a CAL simulation step and novel damage mapping with python scripts. This workflow of simulations provides a complete package for the numerical study of lightning damage tolerance in laminated composites. When combined with a single set of material data and waveform/loading definitions, this approach allows for the individual study and combination of lightning thermal and mechanical damage and residual compressive strength. This workflow of simulations can be considered a step towards a virtual test framework to predict residual compressive strength after lightning strikes.

In Fig. 1, the first step in the sequential analysis procedure is modelling of the thermal-electric behaviour using well established lightning damage models [11,37]. The results from thermal-electric simulations are transferred to structural models to predict lightning mechanical damage (i.e., fibre/matrix failure or delamination), considering strain and heating rates. Finally, the CAL strength is predicted using Abaqus/Explicit with a VUMAT subroutine after damage mapping with python scripts. Each model will now be discussed in more detail.

### 2.2. Material and layup

Herein the simulation workflow will be used to represent a series of experimental tests undertaken by the authors in ref. [35]. Fig. 2a shows the experimental boundary conditions in which a large panel was struck in four quadrants. The specimen was supported between two reinforced stainless-steel frames (underneath and above) with bolts on each short side. This test area was 500 mm × 440 mm resulting in a quadrant size of 275 mm × 250 mm (shown in the blue region in Fig. 2a). Further details of the experimental tests can be found in ref. [35].

The experimental specimens were made using IM7/8552 carbon/epoxy pre-preg. The laminate had a nominal ply thickness of 0.125 mm and quasi-isotropic $[45/90/\text{-}45/0]_{4s}$ stacking sequence, producing a 4

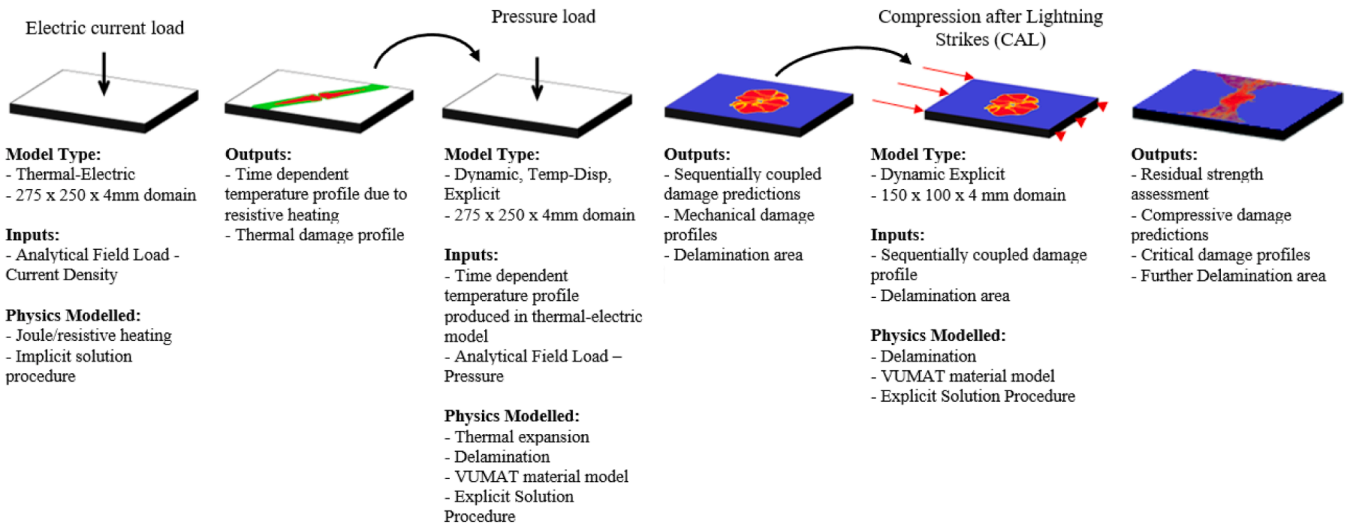


**Fig. 1.** Model flow scheme with corresponding inputs and outputs from literature.

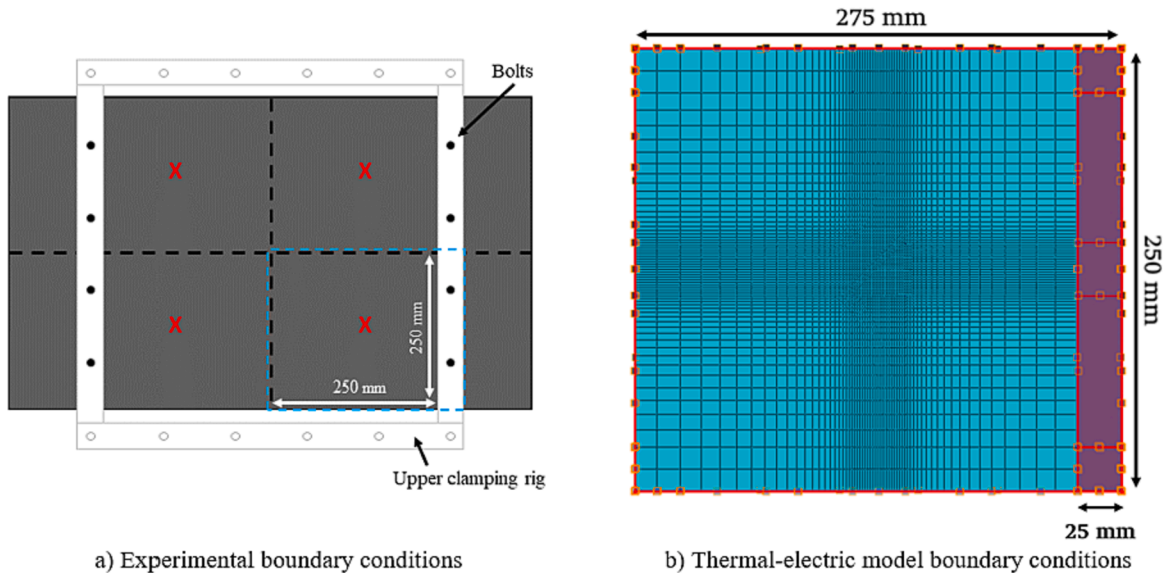


**Fig. 2.** Experimental and thermal-electric model boundary conditions.

mm total thickness. Since there was a lack of published temperature-dependent thermal-electric material properties for the IM7/8552 carbon/epoxy material system, properties were used for a similar material (IM600/133), following the observations of ref. [2], in which it was shown the variation in properties was small. These are shown in Table 1, and can be found in more detail in a published dataset [38]. Mechanical material properties, used in the thermo-mechanical and CAL simulations, are shown in Table 2 [22].

### 2.3. Thermal-electric damage modelling

A thermal-electric finite element (FE) damage model was generated in Abaqus/Standard. Boundary conditions were adapted from the experimental tests [35]. The simulated laminate measured 275 mm × 250 mm × 4 mm. Each specimen was discretised into twenty individual plies on the top and a 1.5 mm thick bulk, homogenised region to make up the remaining specimen thickness at the bottom, since damage was only expected in the upper most plies, close to the top, struck surface. Interlaminar conductivity (or gap conductance), due to contact between neighbouring plies, was included using surface-to-surface contact

**Table 1**
Material properties for thermal-electric damage modelling [38].

| | | Thermal Conductivity (W/mm K) | | |
|---|---|---|---|---|
| Temperature (°C) | Specific Heat (J/kg°C) | Fibre | Transverse | Through-Thickness |
| 25 | 1065 | 0.008 | 0.00067 | 0.00067 |
| 500 | 2100 | 0.00439 | 0.00034 | 0.00034 |
| 800 | 2100 | 0.00261 | 0.00018 | 0.00018 |
| 1000 | 2171 | 0.00174 | 0.0001 | 0.0001 |
| 3316 | 2500 | 0.00174 | 0.0001 | 0.0001 |

| | | Electrical Conductivity (1/ Ω mm) | | |
|---|---|---|---|---|
| Temperature (°C) | Density (kg/mm$^3$) | Fibre | Transverse | Through-Thickness |
| 25 | $1.52x10^{-6}$ | 35.97 | 0.001145 | $1.79x10^{-6}$ |
| 500 | $1.52x10^{-6}$ | 35.97 | 0.001145 | $1.79x10^{-6}$ |
| 800 | $1.10x10^{-6}$ | 35.97 | 0.001145 | $1.79x10^{-6}$ |
| 3316 | $1.10x10^{-6}$ | 35.97 | 0.001145 | $1.79x10^{-6}$ |
| 3334 | $1.11x10^{-9}$ | 35.97 | 2 | $1x10^{6}$ |

**Table 2**
Mechanical properties for thermo-mechanical model and CAL model [22].

| $E_1$ (GPa) | $E_2 = E_3$ (GPa) | $G_{12} = G_{13}$ (GPa) | $G_{23}$ (GPa) | $\nu_{12} = \nu_{13}$ | $\nu_{23}$ | α11 ($^oC^{-1}$) | α22 ($^oC^{-1}$) | α33 ($^oC^{-1}$) |
|---|---|---|---|---|---|---|---|---|
| 161 | 11.4 | 5.17 | 3.98 | 0.32 | 0.44 | 0.0 | $3x10^{-5}$ | $3x10^{-5}$ |
| Xt (MPa) | Xc (MPa) | Yt (MPa) | Yc (MPa) | $S_{12} = S_{13} = S_{23}$ (MPa) | $\Gamma^C_{11}$ (N/mm) | $\Gamma^T_{11}$ (N/mm) | $\Gamma^C_{22}$ (N/mm) | $\Gamma^T_{22}$ (N/mm) |
| 2723 | 1200 | 60 | 200 | 95.8 | 24 | 80 | 0.28 | 1.3 |
| Cohesive Interface Properties | | | | | | | | |
| $t_n^0$(MPa) | $t_s^0 = t_t^0$ (MPa) | $G_n^C$(kJ/m$^2$) | $G_s^C = G_t^C$ (kJ/m$^2$) | | | | | |
| 60 | 90 | 0.2 | 1.0 | | | | | |

[1,39]. The interlaminar thermal conductivity was 500 W/m/K and the electrical conductivity was $1 \times 10^5$ 1/Ω.mm.

Zero electrical potential boundary conditions were applied to the four sides of the specimen. To accurately replicate experimental conditions [35], additional zero potential boundary conditions were applied to 25 mm of the top and bottom surface of one side of the model, where the specimen was clamped, as shown in Fig. 2b. In the experiment [35], metallic bolts were used to ensure tight contact between the specimen surfaces and the grounding clamps. A very small fraction of the induced current may flow through these bolts from the specimen to the grounding clamps. However, the distance from the lightning attachment to the bolts within the grounding upper/lower clamps was approximately 150 mm, thus local current loss through the bolts was minimal. Therefore, the bolts and bolt holes were not considered within the simulations.

Each specimen was meshed with 46,451 DC3D8E elements (8-node linear coupled thermal-electrical brick) with a minimum size of 1.5 mm × 1.5 mm at the lightning attachment point and mesh biasing used at the extremes of the specimen, Fig. 2b, resulting in a mesh-insensitive solution [10,37]. The specimen was loaded using an expanding elliptical arc with an analytical field method, as used in previous work [37], shown in Eqn. (1), where $a$ and $b$ are the major and minor axis lengths of the ellipse, respectively:

$$Field = \left[ \left| \frac{1}{\sqrt{\frac{x^2}{a^2} + \frac{y^2}{b^2}}} \right| \Big/ \left( \left| \frac{1}{\sqrt{\frac{x^2}{a^2} + \frac{y^2}{b^2}}} \right| + 1 \right) \right] \quad (1)$$

Three variants of modified test Waveform D were applied to different specimens with peak currents of 25, 50, and 75 kA, shown in Fig. 3. These current vs time profiles were specified using the amplitude functionality in Abaqus. The total current vs time amplitude profile was divided into individual loads with their own time period. As the arc expanded or moved, new loads were added and old loads were removed as the amplitude was reduced to zero [37,40].

A predefined field was used to set the initial specimen temperature to 25 °C. When current loading was applied to the surface of the specimen, Joule heating occurred due to current flow through the top ply. This Joule heating effect locally increased the temperature of the elements and material degradation resulted. Material degradation was represented by changes in material properties (e.g., temperature dependent conductivity) which was dependent on the temperature history of the material which transitions from virgin polymer properties through to charred polymer properties, ultimately through to fully charred or fully degraded polymer (represented by extremely high electrical conductivity). As a result, more current flowed to neighbouring plies. This process repeats until the end of the simulation producing a prediction of thermal damage in the specimen.

Thermal damage which accumulates in the thermal-electric

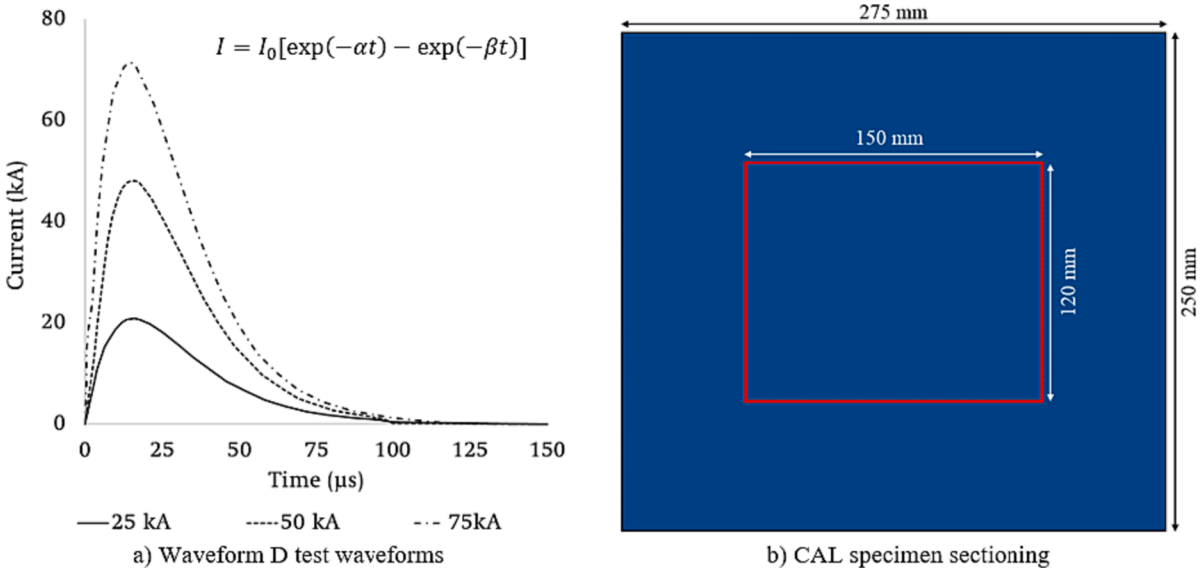


**Fig. 3.** Waveform D test waveforms and CAL specimen sectioning from experimental test panel.

simulations, as a result of Joule heating, is assessed using a temperature criterion, and is characterised as *moderate* or *severe*. To define the moderate and severe damage areas, surface images of experiments were examined and the regions with 'shiny matrix, fibre fracture, matrix cracking and fibre blow out' were manually bounded to define the moderate damage area. For the severe damage area, a single region with a 'deep region of ablated polymer material with char residue, fibre fracture/blow-out' was manually bounded. Moderate thermal damage was correlated with the 300 °C temperature contour representing the onset of epoxy matrix thermal decomposition [37]. Severe thermal damage was correlated with the 500 °C temperature contour (and elements >500 °C), representing the approximate completion of the epoxy matrix thermal decomposition. Fig. 4 compares the areas from the observation of experimental results and the corresponding temperature contours in the relevant simulation. Note that carbon fibres are thermally stable up to ~2000-3000 °C [41], thus any fibre damage (i.e., fracture, blow-out, tow-separation) observed in Fig. 4a is attributed from combined mechanical and thermal loading.

### 2.4. Thermo-mechanical modelling

Thermo-mechanical analysis was completed with a dynamic, temperature-displacement, explicit analysis step in Abaqus/Explicit and could predict lightning mechanical damage due to the combined effects of mechanical strain (from dynamic loading) and thermal strain (due to temperature transferred from the previous thermal damage simulation).

This strain and heating rate dependent failure model used the Hashin failure initiation criteria for both tension and compression in the fibre direction and transverse tension. The Puck [42] criterion was used for compressive failure in the transverse and through-thickness directions. A linear damage evolution law was defined after damage initiation i.e., when the criterion was greater than 0.99. The initiation strain was determined using failure stress and modulus i.e., $\varepsilon_i = X_T/E_{11}$. The failure strain was determined using fracture toughness, strength and the characteristic length ($l^* = \frac{V}{A} \leq \frac{2\Gamma E}{X^2}$, where the variables Γ, E and X are the intralaminar fracture toughness, elastic modulus or strength for the fibre or matrix [43]) of the given element, $\varepsilon_f = 2\Gamma/X_T l^*$. Strain rate effects were included by calculating the rate and then the strain rate regime (quasi-static, intermediate or high-rate). Scale factors based on strain rate were then applied to $E_2$, $E_3$ and the intralaminar strength and fracture toughness properties. Heating rate effects were included by offsetting the temperature at which the moduli and strength of the material changed. Further details of the development of this model and its implementation are given in ref. [16].

The temperature profile from each node of each element of the FE mesh in the thermal-electric simulation was passed to an equivalent thermo-mechanical model using Python scripts, as discussed in previous works [16,17]. Thus, the temporal variation in temperature is represented throughout the duration of the thermo-mechanical simulation when predicting total lightning damage in the simulated laminates. C3D8RT (8-node trilinear displacement and temperature, reduced integration with default hourglass control) elements were used in each thermo-mechanical simulation [44] with material behaviour controlled by the strain and heating rate dependent failure model developed in ref. [16]. Pressure loading was applied to the specimen using the same analytical field method with arc expansion as in Section 2.3.

To determine the lightning-induced dynamic mechanical loading from the peak current waveform, a conversion procedure was used. Lee et al. [3,45] proposed a simple conversion procedure from a peak current amplitude to equivalent lightning shockwave overpressure and provided a conversion table. Note that lightning mechanical damage in the structure is associated with two primary sources (i.e., shockwave overpressure and electromagnetic pinch pressure/force) but shockwave overpressure is most dominant [45]. Fig. 5a shows the magnitude of equivalent lightning mechanical loading as a function of the peak amplitude of a current impulse waveform. In this work, the magnitudes of mechanical loading corresponding to 25, 50, and 75 kA peak currents, were calculated as 4.7, 8.0, and 11.4 MPa, respectively. Fig. 5b shows the dynamic lightning mechanical loading which was assumed to follow identical temporal characteristics of the current waveforms (Fig. 3a).

Delamination between neighbouring plies was captured using cohesive surfaces with a bi-linear traction-separation law [16]. The onset of interfacial damage was governed by the quadratic stress criterion, and fracture energy dissipation during damage propagation was governed by the Benzeggagh and Kenane (B-K) criterion [13,46]:

$$G^C = G_n^C + \left(G_s^C - G_n^C\right)\left(\frac{G_s + G_t}{G_n G_s + G_t}\right)^{\eta_{BK}^C} \quad (2)$$

where $\eta_{BK}^C$ is the mixed-mode interaction property and $G_n^C$ and $G_s^C$ are the critical fracture energies required to cause failure in the normal and shear directions, respectively.

The same regions of each specimen were constrained in terms of both electrical and mechanical clamping in the relevant experiments. Therefore, the previous electrical potential boundary conditions were converted to mechanical boundary conditions. Therefore, in the case of

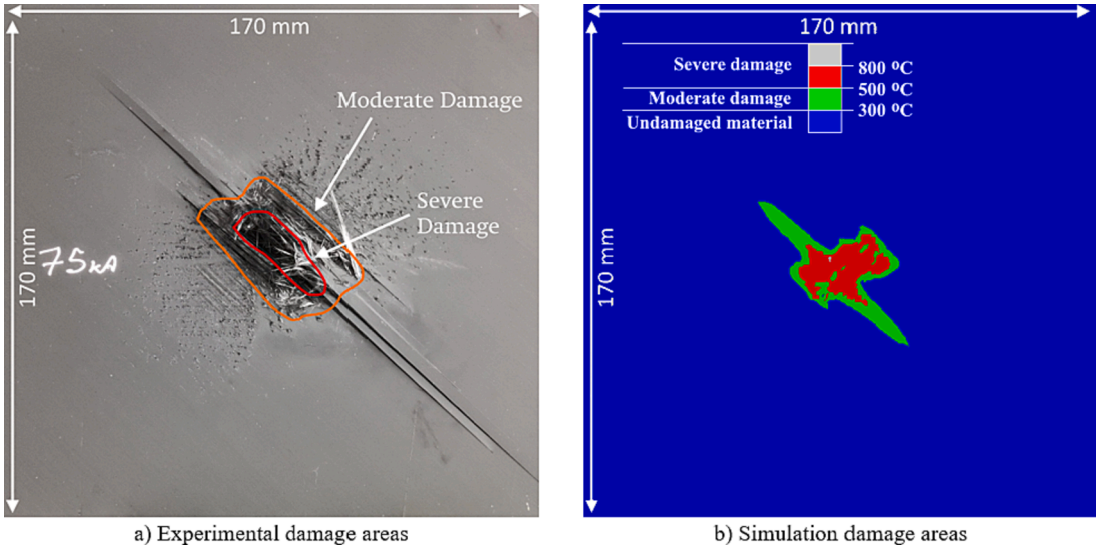


a) Experimental damage areas b) Simulation damage areas

**Fig. 4.** Experimental damage areas and simulation temperature contours.

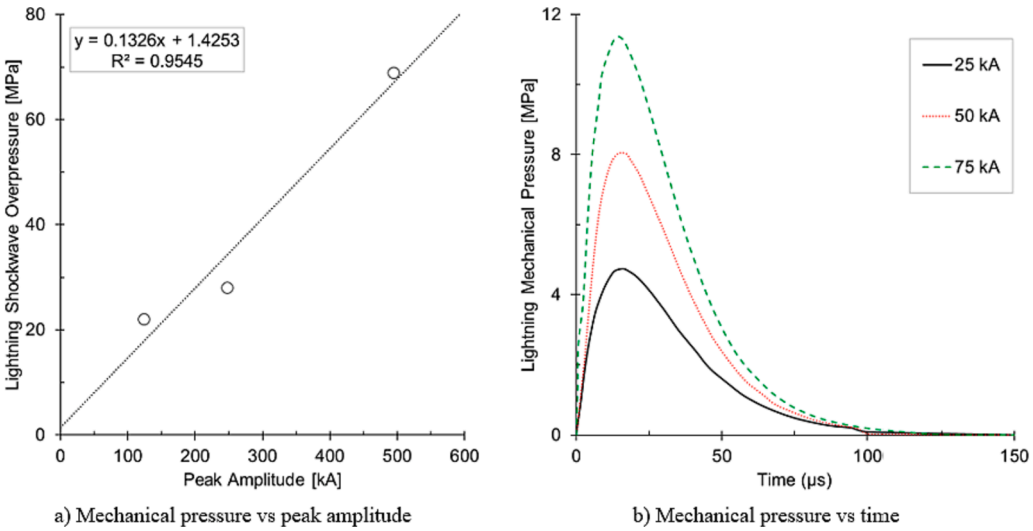


**Fig. 5.** Graphs of conversion from peak current amplitude to lightning mechanical pressure.

the thermo-mechanical simulations, the regions shown in Fig. 2b, were constrained in all directions to replicate the clamping arrangement used in the corresponding experiments [35].

### 2.5. Compression after lightning strike (CAL) modelling for residual strength

The final simulation step, CAL simulation, was completed using Abaqus/Explicit. The models for the study of CAL residual strength follow exactly the same specimen dimensions used in the corresponding experiments [35], which were sectioned from the main lightning strike experimental quadrants as shown in Fig. 3b. Therefore, the in-plane dimensions of the simulated laminates were reduced to 150 × 120 mm. In this analysis the element type was changed to C3D8R (8-noded continuum elements, reduced integration with default hourglass control). The FE mesh in the CAL models was different from that used in lightning simulations and had a uniform size of 1.5 × 1.5 mm across its length and width. This uniform mesh would allow the location of failure to change and avoid a localising effect that could be caused by local mesh refinement. The uniform mesh could also better capture the stress distribution at the boundaries. A simple mesh study was completed on the 25kA case and found that varying the element size had little effect on the predicted CAL strength. For example, a 0.75 mm × 0.75 mm mesh predicted a CAL strength of 336 MPa while the 1.5 mm × 1.5 mm mesh predicted a CAL strength of 334 MPa. At most the CAL strength varied by ≤ 1% with changes to the mesh. Therefore, based on this mesh study, a 1.5 mm × 1.5 mm mesh was chosen across all models for easy comparison and improved computational performance.

The elastic constants, strengths, and interfacial/cohesive properties used in this model are shown in Table 2. Given the damage in the lightning models was confined to the upper plies and in the interests of minimising simulation run-time, the CAL models were also discretised into individual plies on the top and a thick bulk, homogenised region to make up the remaining specimen thickness. Multiple elements were used through the thickness of the bulk region to account for bending behaviour. Two sets of material data were used. One set was used for ply failure in the upper individual plies while composite laminate theory (and experimental data in literature [47]) was used to determine the homogenised properties of the bulk region.

The compressive failure criterion used herein was a simple maximum stress criterion with the inputs from the open literature in Table 2:

$$F_1^c = \frac{|\sigma_1|}{X_c} \geq 1 \tag{3}$$

When the maximum fibre-direction compressive stress ($\sigma_1$) reaches the critical value ($X_c$), the elements are flagged, and their fibre-direction stress in the individual plies or loading direction stress in the bulk region is reduced to zero. This was found to be sudden by nature with the blunt lightning damage, hence no attempt was made to capture stable kink band propagation. The ultimate failure of the model was not determined by the timing of the flagged "first failure" but by the peak load in the stress-displacement graph, though the two events were very closely related. Further delamination was captured in this model using the same approach as the thermo-mechanical models in Section 2.4.

#### 2.5.1. Variation of CAL boundary conditions

The recently published work on CAL testing [35] demonstrated that the failure of the 25 kA case developed from the centre of the specimen. Therefore, this case will be used for verification of the 25 kA model. It was also found that for higher peak currents (50 and 75 kA) compression failure did not initiate at the lightning damage area (central failure), rather failure occurred at the test boundary conditions (edge failure), due to the unsupported gap in the CAI jig, Fig. 6a. Therefore, two simulations were completed for each 50 and 75 kA case, using the boundary conditions derived from the preceding experimental work [35]. The simulations with the unsupported gap (Fig. 6c) could then be correlated with the experimental results from ref. [35]. The simulations without the unsupported gap (Fig. 6d) could be used to better understand the effect of the unsupported gap on CAL residual strength. A summary of these simulations and their purpose is presented in Table 3 where NGCF refers to the cases with no unsupported gap leading to central failure around the lightning attachment point and UGEF indicates the presence of an unsupported gap leading to edge failure at the test boundary conditions.

### 2.6. Transfer of damage between simulations

The models used herein, required different specimen sizes Fig. 3b and mesh densities (Fig. 2b and Fig. 6c) depending on the physics being studied. Therefore, it was important to develop a simple, but robust strategy to transfer damage from one mechanical simulation to the next (i.e. thermo-mechanical lightning simulation to CAL simulation). Two forms of damage, mechanical damage to the ply (intralaminar) and delamination (interlaminar) were transferred using Python scripts. Mechanical damage was transferred by analysing areas of element deletion on each ply, which represented the hole produced in the specimen, following the thermo-mechanical analysis, shown in Fig. 7a for the first ply. Nodal coordinates were extracted to describe the hole,

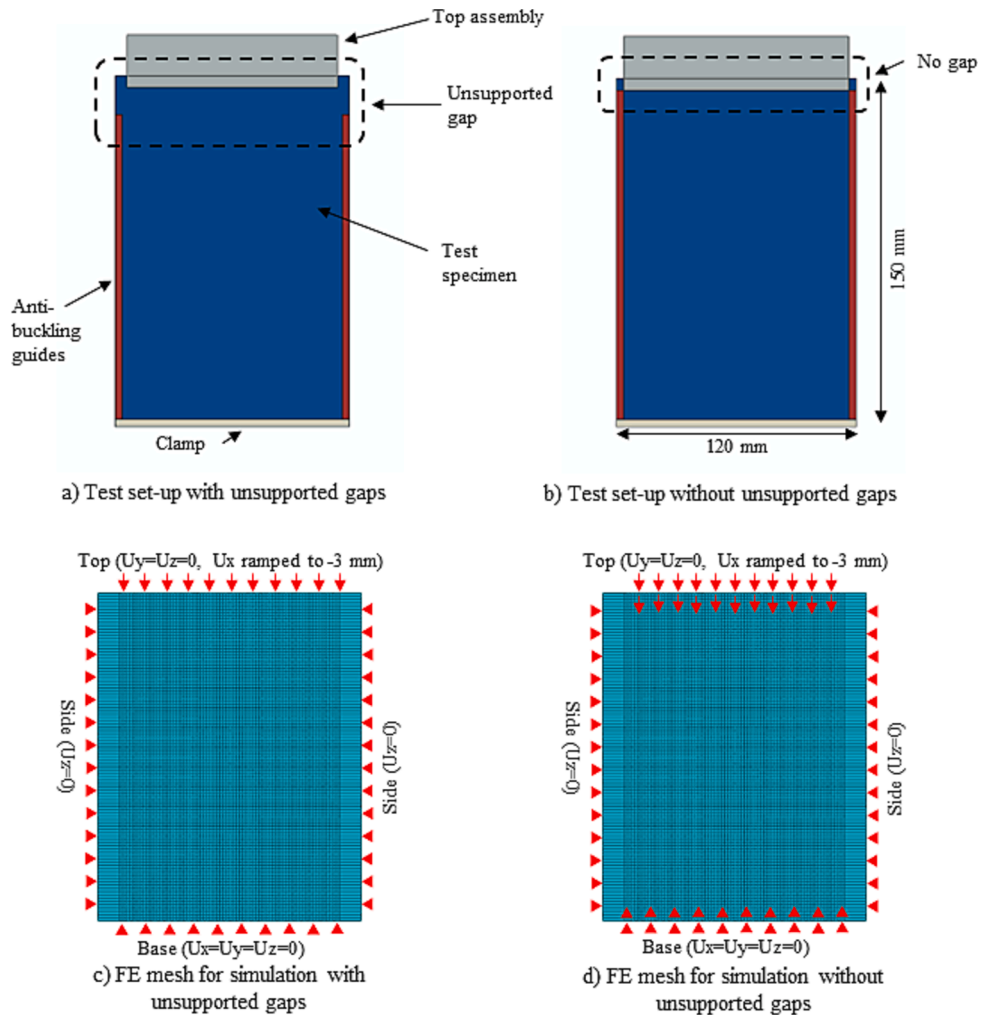


**Fig. 6.** The CAL FE model with the boundary conditions labelled.

**Table 3**
CAL simulation variations.

| Peak current (kA) | Boundary Conditions | Purpose |
|---|---|---|
| 25 | NGCF | Experimental verification |
| 50 | UGEF | Experimental verification |
| 50 | NGCF | Boundary condition variation |
| 75 | UGEF | Experimental verification |
| 75 | NGCF | Boundary condition variation |

converted to create element sets and transferred to make equivalent element sets within the CAL model, shown in red in Fig. 7b. Some loss of damage area occurred transferring from one model to the next but this was analysed and was around 2–3%. Since the difference was small, this reconstructed (or mapped) damage in the CAL analysis reasonably captures lightning thermal and mechanical damage areas. The elements in this set were then assigned near-zero mechanical properties to avoid potential computational errors due to zero stiffness specification. A second element set was created on each ply to represent undamaged regions and were assigned pristine mechanical properties.

As mentioned, delamination was captured using cohesive surfaces in the CAL simulations. Delamination was transferred by analysing the CSDMG area (scalar damage variable for delamination) from the thermo-mechanical analysis for each ply-ply interface. A similar procedure was used as before to create element sets and then corresponding surfaces. The *SurfaceFromElsets* functionality was used to create the relevant delaminated and pristine surfaces. Therefore, delaminated surface areas were assigned near-zero stiffness while corresponding pristine surface areas were assigned properties as shown in Table 2.

## 3. Results

The extent of lightning damage is grouped in three broad categories based on either temperature contours or deleted elements; moderate thermal damage, severe thermal damage, and mechanical damage.

Moderate and severe thermal damage have been determined visually from the experiments for each peak current. Fig. 8 shows the moderate (orange) and severe (red) thermal damage areas highlighted for each of the 25, 50, and 75 kA test specimens. In the 25 and 50 kA cases, moderate and severe thermal damage could not be easily differentiated from the top-down photographs using image binarisation techniques. Therefore, only moderate thermal damage is highlighted for these cases.

In thermo-mechanical simulations, moderate and severe thermal damage can still be assessed. However, inter-ply delamination and mechanical damage, resulting from the combination of mechanical and thermal strains are more relevant. Mechanical damage has been defined to represent the hole produced in the specimen due to the combined effects of thermal and mechanical loading, illustrated by deleted elements in the simulation.

In CAL simulations, further delamination can be predicted under compressive loading, as can compressive failure initiation. Residual stress values (in MPa) were calculated from the peak compressive force (in N) divided by the gross-section area. A summary of the predicted

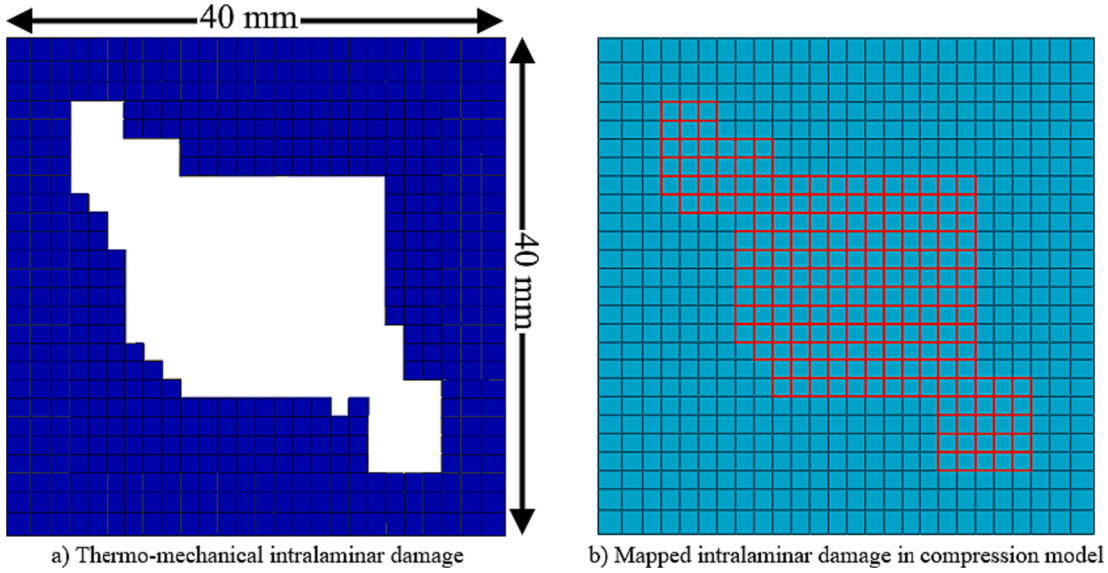


**Fig. 7.** Comparison of a) thermo-mechanical damage and b) mapped damage region on compression model.

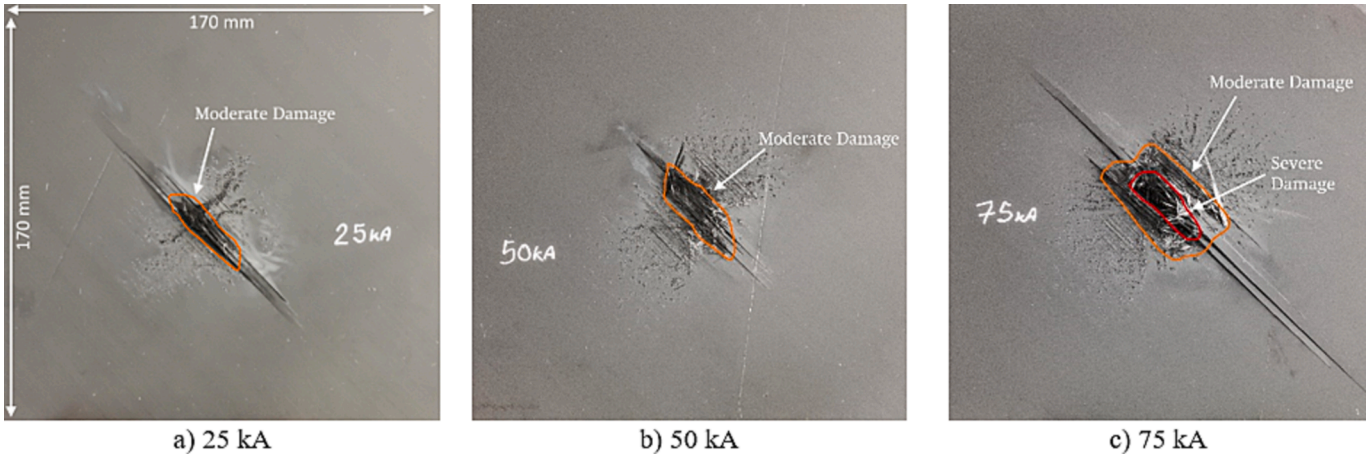


**Fig. 8.** Highlighted moderate and severe damage areas on different test specimens [35].

damage in all simulations along with relevant measured experimental values are provided in Table 4.

### 3.1. Thermal-electric and thermo-mechanical results

#### 3.1.1. Thermal-electric results

Initially current applied to the top surface of the specimen flowed predominantly in the fibre direction (the optimal conduction path). However, some current flowed in the transverse and through thickness directions due to the difference in conductivity in each direction. Note that electrical conductivity in the fibre direction is much higher than in the transverse or through thickness directions. As the temperature of the top ply increased, due to Joule heating, matrix thermal decomposition occurred and through-thickness conductivity drastically increased which allowed current to reach the second ply and beyond. This behaviour created a pattern of damage through the specimen thickness based on the fibre orientation of each ply. Since less current flowed into each subsequent ply, the size of the damaged area reduced with each ply through the specimen thickness.

Thermal-electric results are summarised in Table 4. Fig. 9 shows predicted temperature contours overlaid on the lightning damage in carbon/epoxy composite laminate subjected to 25, 50, and 75 kA peak

**Table 4**
Damage results summary.

| | | Experiments | | | Simulations | | |
|---|---|---|---|---|---|---|---|
| | | 25 kA | 50 kA | 75 kA | 25 kA | 50 kA | 75 kA |
| Thermal-electric model(s) | Moderate Thermal Damage Area ($mm^2$) | 791 | 1461 | 1606 | 795 | 1333 | 1506 |
| | Severe Thermal Damage Area ($mm^2$) | – | – | 437 | 164 | 623 | 725 |
| | Damage Depth (plies/mm) | 4 / 0.5 | – | – | 4 / 0.5 | 9 / 1.125 | 11 / 1.375 |
| Thermo-mechanical model(s) | Critical Damage Area ($mm^2$) | – | – | – | 438 | 932 | 1071 |
| | Critical Damage Volume ($mm^3$) | – | – | – | 122 | 622 | 752 |
| | Delamination Area ($mm^2$) | – | – | – | 955 | 1426 | 1409 |

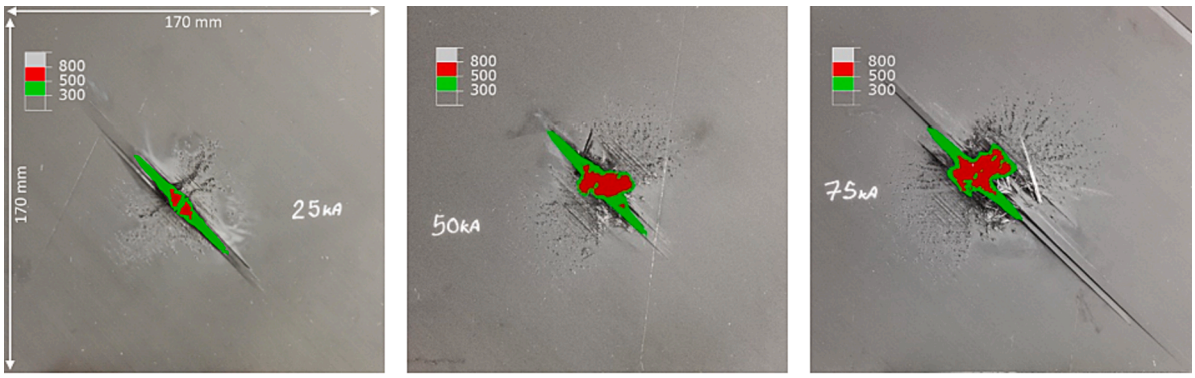


**Fig. 9.** Comparison of experimental damage and thermal-electric simulation predictions (green contour represents moderate thermal damage, red contour represents severe thermal damage). (For interpretation of the references to colour in this figure legend, the reader is referred to the web version of this article.)

current tests from ref. [35] and can be compared with the experimental damage in Fig. 8. In the 25 kA case, the experimental moderate damage area was approximately 791 mm$^2$ (orange region on Fig. 8a). The predicted moderate damage was within 1% of the experimental area at 795 mm$^2$ (green region on Fig. 9a). The predicted severe damage area was 164 mm$^2$. The predicted damage penetration was up to the fourth ply (0.5 mm).

Fig. 10 shows the highlighted thermal damage in each ply through the thickness of the 25 kA test specimen, outlined manually in green, and the corresponding thermal damage predicted in the thermal-electric simulation, represented by temperature contours. The green lines on the experimental CT images outline the moderate damage area. It can be seen that there is good correlation between the simulation temperature contours and the CT scans, in particular in plies one and two. However, there is less correlation between the thermal contours in plies 3 and 4 and the CT scans.

In the 50 kA case, the experimental moderate damage area was approximately 1461 mm$^2$. The predicted moderate damage was within 9% of the experimental area at 1333 mm$^2$, while the predicted severe damage area was 623 mm$^2$. The predicted damage depth was nine plies (1.125 mm). In the 75 kA case, the experimental moderate and severe damage areas were 1606 mm$^2$ and 437 mm$^2$, respectively. The predicted moderate damage area was 1506 mm$^2$ (within 7%), while the predicted severe damage area was 725 mm$^2$ (within 40%). The predicted damage depth was twelve plies, 1.5 mm.

### 3.1.2. Thermo-mechanical results

Fig. 11 compares the X-ray Computed Tomography (CT) images from Xu et al. [35] with the lightning mechanical damage predictions, from the thermo-mechanical simulations, at the centre of each specimen for the three peak currents. In this figure, the coloured regions represent delamination while the deleted elements represent mechanical damage, which describes the hole produced in the specimen due to the combined effects of thermal and mechanical loads.

In the 25 kA case, mechanical damage, which represents the hole produced in the specimen due to the combined effects of thermal and mechanical loads was 438 mm$^2$, defined as an area of deleted elements. This mechanical damage area corresponded to a damage volume of 122 mm$^3$. The predicted delamination area and depth were 955 mm$^2$ and 0.625 mm (up to the 5th ply), respectively which were 20% and 25% greater than the moderate thermal damage area and depth.

In the 50 kA peak current case, the mechanical damage area for the 50 kA case was 932 mm$^2$ while the mechanical damage volume was 622 mm$^3$. The delamination area increased by 50% from the 25 kA case to 1426 mm$^2$.

In the 75 kA case, the mechanical damage area for the 75 kA case was 1071 mm$^2$ while the mechanical damage volume was 752 mm$^3$. The delamination area was within 2% of the 50 kA case.

## 3.2. CAL residual strength results

Fig. 12 shows the predicted CAL strengths, and those obtained from the CAL tests [35], for all three peak currents and both boundary

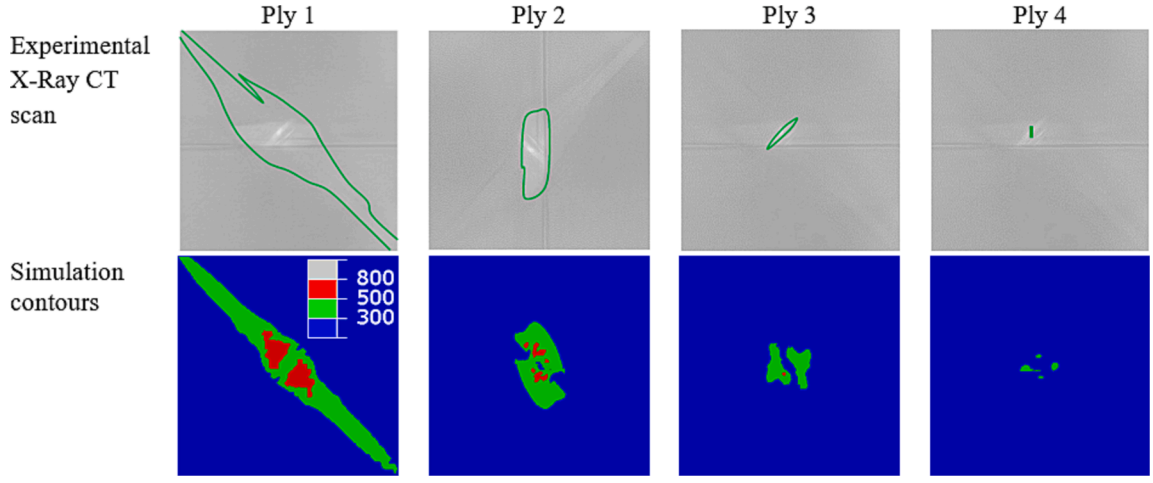


**Fig. 10.** Predicted ply-by-ply temperature contours compared with experimental C-scan observations from ref. [35] for 25 kA peak current (units on simulations = °C).

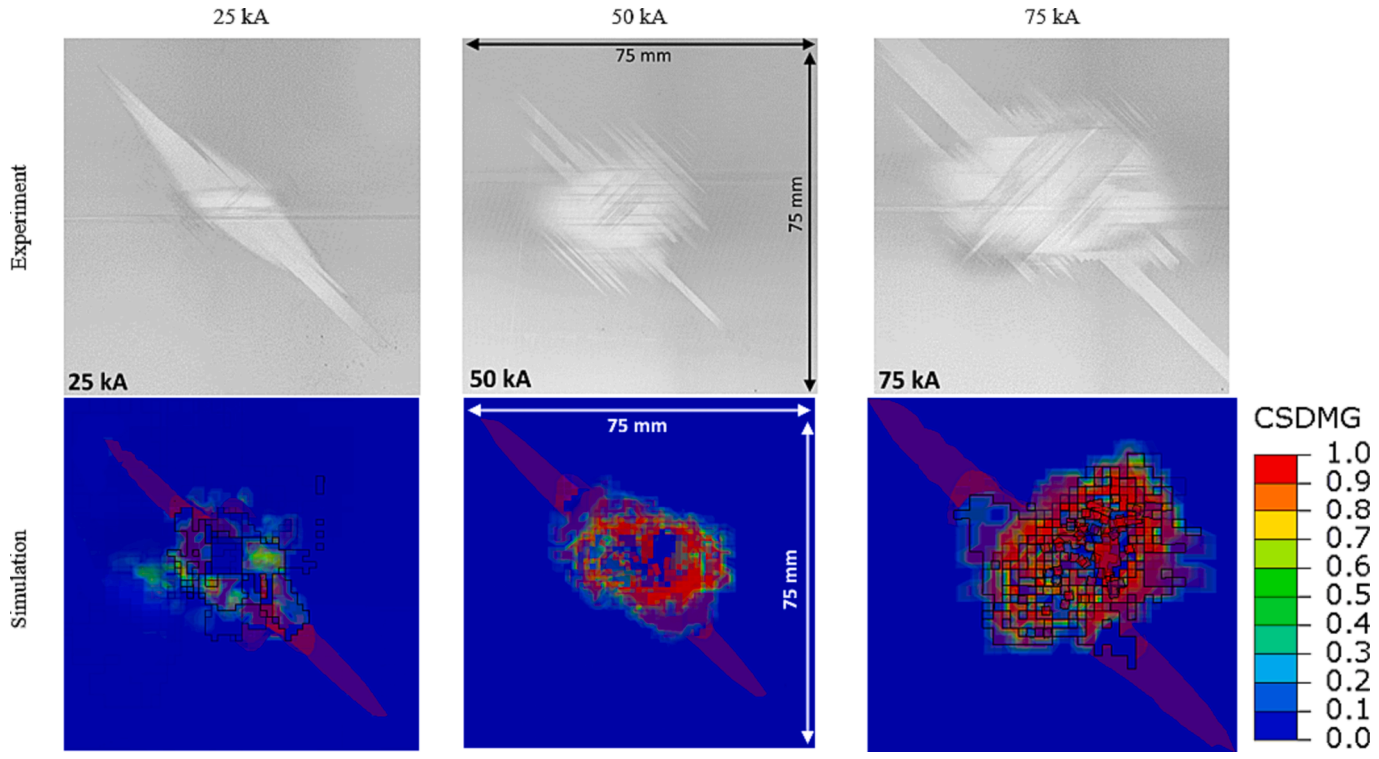


**Fig. 11.** Comparison of experimental X-ray Computed Tomography (CT) and thermo-mechanical damage predictions (colours represent delamination area).

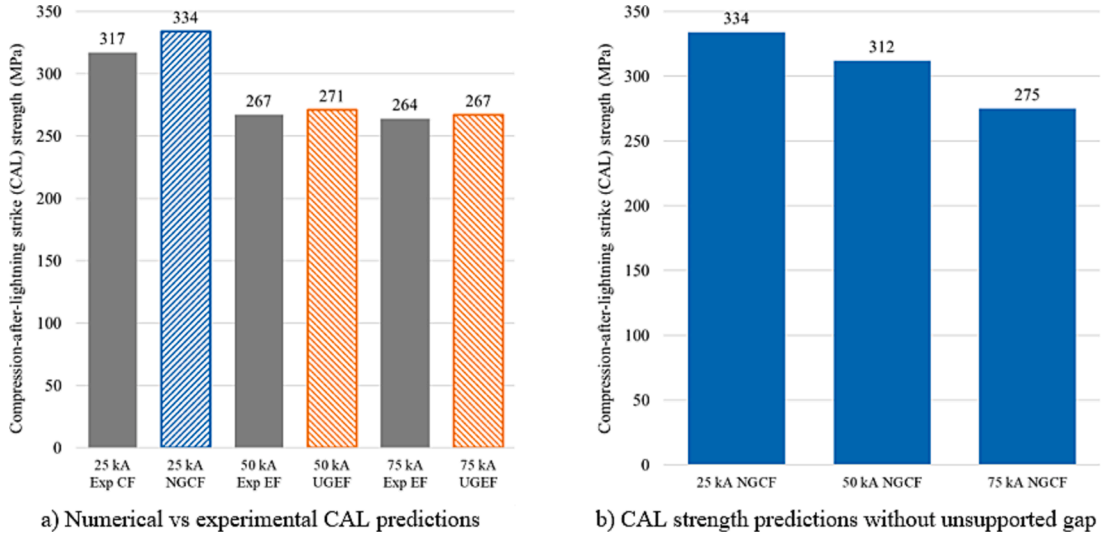


**Fig. 12.** Comparison of CAL strengths for experimental specimens from ref. [35] and different simulation predictions (NGCF = no gap, central failure, UGEF = unsupported gap, edge failure).

conditions. Fig. 12a compares the experimental CAL strength and the corresponding simulation with varying boundary conditions to match the experiments. Fig. 12b compares the predicted CAL strength versus peak current with fixed boundary conditions. In these figures, NGCF refers to the cases with no unsupported gap leading to central failure around the lightning attachment point. UGEF indicates the presence of an unsupported gap leading to edge failure at the test boundary conditions.

Comparing the results for the 25 kA model the CAL strength prediction (334 MPa) was within 6% of the experimental result (317 MPa). The CAL modelling results for 50 and 75 kA peak currents (incorporating the unsupported gap, leading to edge failure) are shown in orange in Fig. 12a and agree well with the corresponding experiments, both within 2%. In the 50 kA case, the predicted CAL strength was 271 MPa while the experimental CAL strength was 267 MPa (within 1.5%). In the 75 kA case, the predicted CAL strength was 267 MPa while the experimental CAL strength was 264 MPa (within 1.2%).

The results for 25, 50, and 75 kA peak currents without the unsupported gap (NGCF) are shown in Fig. 12b. The models captured a change of failure mode from undesirable edge failure to central failure, around the lightning attachment and damage zone, when eliminating the gap between the loading edges and the end of anti-buckling constraints. This agrees with the experimental observation and confirms the effectiveness of the CAL test design recommendation in Xu et al. [35]. The predicted

CAL strength of the 50 kA without the gap was 312 MPa, 14% higher than the result with the unsupported gap. A similar observation was seen in the 75 kA case, 275 MPa without the gap, 3% higher than the result with the unsupported gap.

The change of failure mode from central to edge failure, associated with the change in boundary conditions is shown in Fig. 13. The delamination profile, from superimposed interfacial damage from all ply interfaces, and predicted compressive failure initiation are shown for both failure modes following a 50 kA strike. When the unsupported gap was removed (Fig. 13a and c), the specimen failed at its centre and delamination propagated from the existing lightning strike delamination to the specimen edges.

However, when the unsupported gap was included (Fig. 13b and d), the specimen failed at the edges. In this case delamination occurred at the loading grip. The existing lightning strike delamination, resulting from lightning mechanical loading and neglecting compressive CAL loading, did not propagate further.

### 3.3. Correlating lightning damage with CAL strength

The results produced herein significantly allow for the relationships between different lightning damage types and CAL strength to be established. Fig. 14a shows a strong linear relationship between the lightning peak current and the CAL strength, which is in excellent agreement with similar works in literature [20,21], with an $R^2$ value of 0.99. Fig. 14b shows the relationship between the predicted area of different lightning damage types (severe thermal damage, mechanical damage and delamination) and the resulting CAL strength. Strong linear relationships are observed between each damage type and the CAL strength. Mechanical damage produced in the thermo-mechanical simulation, due to the combined effects of mechanical strain (from dynamic loading) and thermal strain (due to Joule heating), had the greatest correlation ($R^2 = 0.82$). Delamination area had the lowest correlation of these three damage types, $R^2 = 0.61$. Severe thermal damage, as a result of Joule heating, had the second greatest correlation, $R^2 = 0.79$, since this represents areas of complete matrix decomposition. Moderate thermal damage, partial matrix decomposition, not shown

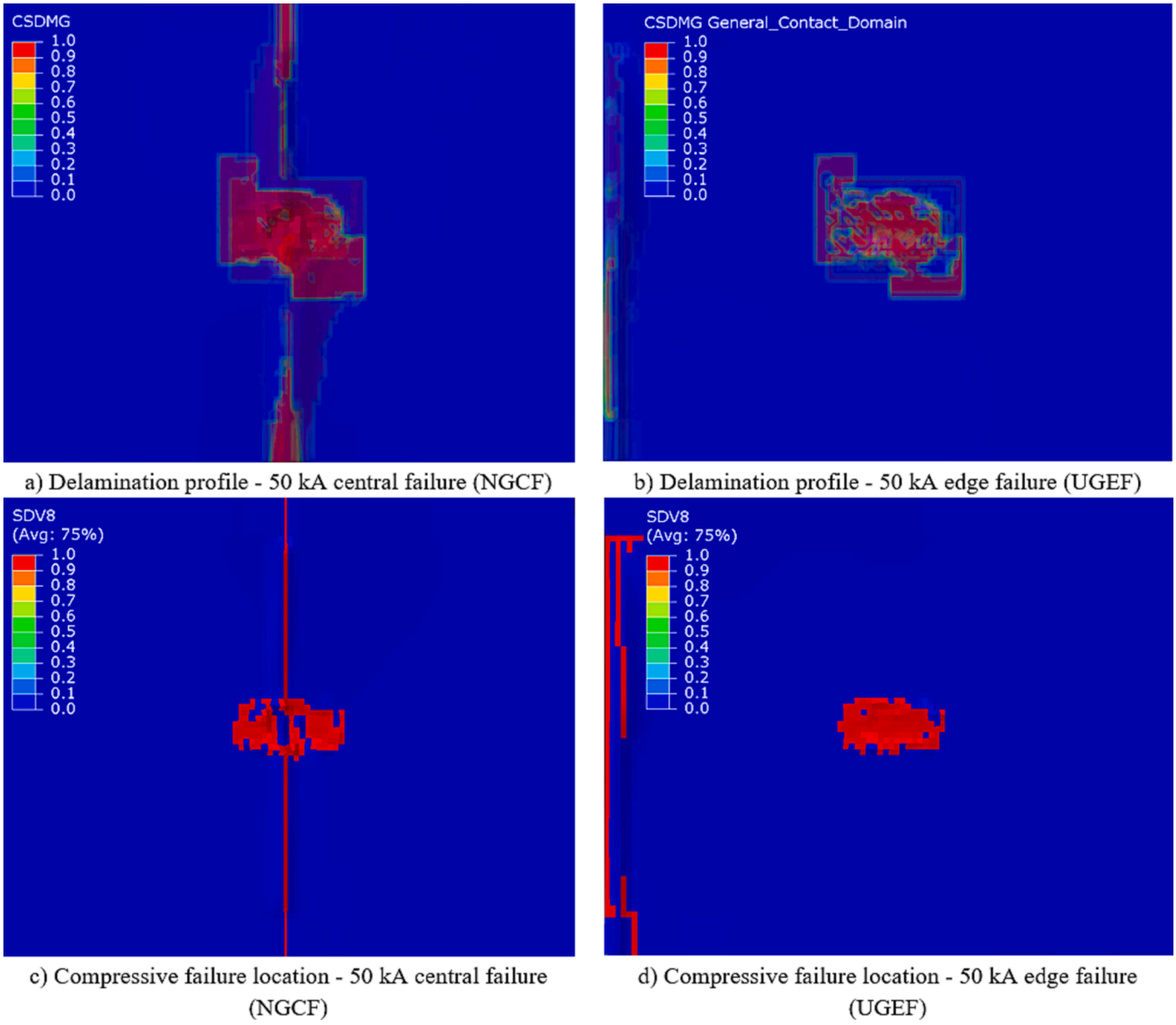


**Fig. 13.** Delamination and compressive failure locations for different failure modes after 50 kA strike (where red represents failed elements). (For interpretation of the references to colour in this figure legend, the reader is referred to the web version of this article.)

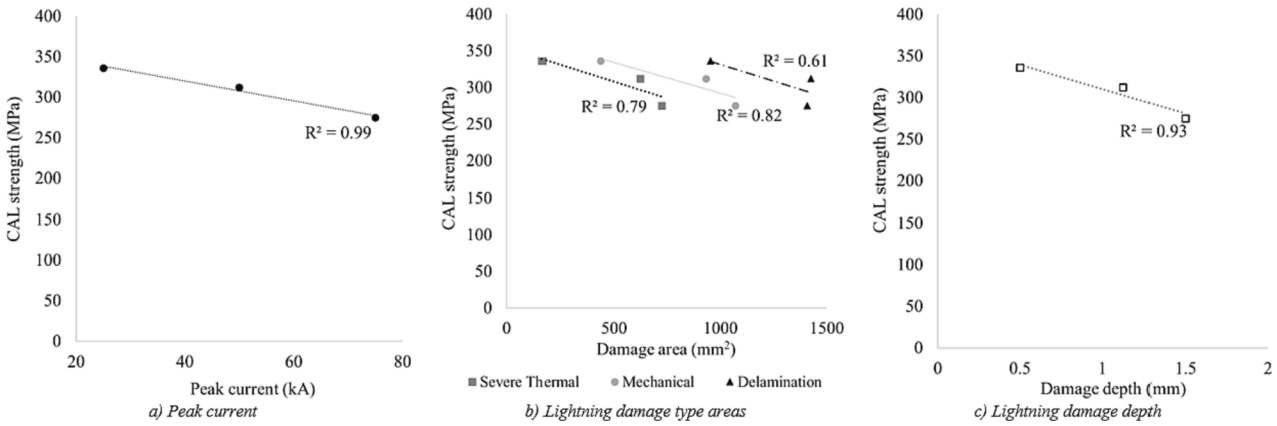


**Fig. 14.** Relationship between CAL strength and a) peak current, b) lightning damage areas and c) lightning damage depth.

here for brevity, had an $R^2 = 0.84$. Damage depth had a correlation of $R^2 = 0.93$ with CAL strength, Fig. 14c. This is likely due to the number of damaged plies, in particular 0° plies, through the specimen thickness. 0° plies align with the compressive loading direction and there is one damaged 0° ply at 25 kA peak current but two damaged 0° plies at 50 kA peak current.

### 3.4. Results discussion

The experiments conducted in ref. [35] demonstrated that the standard CAI test setup had the potential for CAL application. However, careful modifications are required depending on the peak amplitude of the applied lightning current waveform. The models presented herein have created a simulation workflow which could form the basis of a virtual test framework to predict thermal damage, mechanical damage, and inter-ply delamination, and the resulting CAL strength for an artificial lightning strike. These virtual tests have the potential to reduce the need for expensive lightning strike tests and residual strength experiments given these high-fidelity simulations have been well-verified in a variety of cases.

The component parts of this virtual test framework have been previously applied to a number of different waveforms (A and B) [16], layups ($[45/0/-45/90]_{4s}$ and $[45/90/-45/0]_{4s}$) [40], and boundary conditions (two edges clamped to a base, four edges clamped to a base, and the specimen placed on a surface) [11]. Indeed, the existing workflow, without the addition of a CAL simulation step, has been applied at different levels of analysis (mesoscale and microscale) [16,48].

However, to-date, validation is only based on a comparatively small number of experimental tests and to have complete confidence in the virtual test framework, further, significant physical validation would be required.

The models presented herein have been validated against the relevant experiments. For example, it was shown that all models produced CAL residual strength predictions within 6% of each experimental result even with a change in boundary conditions and failure mode. The models therefore can help point to the direction of improvements in future experiments such as determining the transition lightning current from the undesirable edge failure to central failure near the strike site.

The models herein, have also established the correlation between different lightning damage types and the resulting CAL strength. Mechanical damage due to the combined effects of mechanical and thermal strains had the greatest correlation while in this study lightning strike induced delamination was relatively weakly correlated. Peak current has a strong correlation to residual strength, a relationship seen in other works [20,21].

## 4. Conclusions

This work has conducted a comprehensive modelling study and assessment of the Compression after Lightning Strike (CAL) residual strength of composite laminates exposed to 25, 50 and 75 kA peak current variants of test Waveform D. Two existing and established lightning strike simulation techniques, thermal-electric and dynamic, temperature-displacement, explicit analyses, have been combined with a CAL modelling methodology to create a virtual test framework and to determine the expected strength knock-down due to combined thermal and mechanical lightning damage and different CAL boundary conditions.

The requirements of this virtual test framework were to accurately predict thermal damage, inter-ply delamination and mechanical damage, and the resulting CAL strength. Lightning strike models were compared with experimental results in terms of predicted damage and were shown to capture moderate thermal damage areas within 9% of the experimental damage. Thermo-mechanical models were then completed to predict the damage profile (both mechanical damage and delamination) due to combined thermal (Joule heating) and mechanical (shock-wave overpressure) loading and resulting mechanical and thermal strains. These damage profiles were transferred to a CAL model using a novel lightning damage mapping technique using python scripts. The residual CAL strength was predicted using a maximum stress failure criterion for ply failure, combined with cohesive surfaces for delamination. Together with the simulated lightning damage, this modelling framework could predict the residual CAL strength within 6% of the experimental values after 25, 50, and 75 kA peak current strikes. The model was also able to capture the change of failure mode at higher peak currents when considering boundary condition modifications in the CAL experimental test.

This work has also established the link between individual lighting damage morphologies and the resulting CAL strength. It has been shown that, mechanical damage to the individual plies, due to the combined effects of mechanical and thermal strains during the strike had a significant effect on CAL strength, $R^2 = 0.82$. The current modelling framework provides a complete numerical solution for predicting CAL strength, potentially reducing the need for expensive lightning and residual strength experiments.

While the proposed framework was successfully validated for three peak current cases with a single material type and layup, further verification with different layups and boundary conditions would enhance the usage of this framework as a virtual test tool. However, given the extensive previous application of component parts of this framework to other problems (considering different layups, boundary conditions, waveforms and length scales) this work presents a pathway towards a virtual test framework. It can also accelerate the design of lightning resistant and damage tolerant composite structures.

## CRediT authorship contribution statement

**S.L.J. Millen:** Methodology, Software, Validation, Formal analysis, Investigation, Writing – original draft, Visualization. **X. Xu:** Methodology, Software, Validation, Formal analysis, Investigation, Writing – original draft, Visualization. **J. Lee:** Resources, Writing – review & editing. **S. Mukhopadhyay:** Software, Writing – review & editing. **M.R. Wisnom:** Writing – review & editing. **A. Murphy:** Writing – review & editing.

## Declaration of Competing Interest

The authors declare that they have no known competing financial interests or personal relationships that could have appeared to influence the work reported in this paper.

## Data availability

Data will be made available on request.

## Acknowledgements

This research did not receive any specific grant from funding agencies in the public, commercial, or not-for-profit sectors.

## References

[1] Millen SLJ, Murphy A. Modelling and analysis of simulated lightning strike tests: a review. Compos Struct 2021;274. https://doi.org/10.1016/j.compstruct.2021.114347.
[2] Millen SLJ, Ashworth S, Farrell C, Murphy A. Experimental effects of heating rate on material properties for lightning strike simulations. Compos B Eng 2022;228. https://doi.org/10.1016/j.compositesb.2021.109438.
[3] Lee J, Lacy TE, Pittman CU. Coupled thermal electrical and mechanical lightning damage predictions to carbon/epoxy composites during arc channel shape expansion. Compos Struct 2021;255:112912. https://doi.org/10.1016/j.compstruct.2020.112912.
[4] Lee J, Lacy TE, Pittman CU. Lightning mechanical damage prediction in carbon/epoxy laminates using equivalent air blast overpressure. Compos B Eng 2021;212. https://doi.org/10.1016/j.compositesb.2021.108649.
[5] Harrell TM, Madsen SF, Thomsen OT, Dulieu-Barton JM. On the effect of dielectric breakdown in UD CFRPs subjected to lightning strike using an experimentally validated model. Appl Compos Mater 2022. https://doi.org/10.1007/s10443-022-10014-7.
[6] Dong Q, Wan G, Guo Y, Zhang L, Wei X, Yi X, et al. Damage analysis of carbon fiber composites exposed to combined lightning current components D and C. Compos Sci Technol 2019;179:1–9. https://doi.org/10.1016/j.compscitech.2019.04.030.
[7] Guo Y, Xu Y, Wang Q, Dong Q, Yi X, Jia Y. Enhanced lightning strike protection of carbon fiber composites using expanded foils with anisotropic electrical conductivity. Compos A Appl Sci Manuf 2018;117:211–8. https://doi.org/10.1016/j.compositesa.2018.11.022.
[8] Kumar V, Yokozeki T, Okada T, Hirano Y, Goto T, Takahashi T, et al. Effect of through-thickness electrical conductivity of CFRPs on lightning strike damages. Compos A Appl Sci Manuf 2018;114:429–38. https://doi.org/10.1016/j.compositesa.2018.09.007.
[9] Li Y, Li R, Lu L, Huang X. Experimental study of damage characteristics of carbon woven fabric/epoxy laminates subjected to lightning strike. Compos A Appl Sci Manuf 2015;79:164–75. https://doi.org/10.1016/j.compositesa.2015.09.019.
[10] Shah SZH, Lee J. Stochastic lightning damage prediction of carbon/epoxy composites with material uncertainties. Compos Struct 2022;282. https://doi.org/10.1016/j.compstruct.2021.115014.
[11] Millen SLJ, Murphy A. Understanding the influence of test specimen boundary conditions on material failure resulting from artificial lightning strike. Eng Fail Anal 2020;114. https://doi.org/10.1016/j.engfailanal.2020.104577.
[12] Fu K, Ye L. Modelling of lightning-induced dynamic response and mechanical damage in CFRP composite laminates with protection. Compos Struct 2019;218:162–73. https://doi.org/10.1016/j.compstruct.2019.03.024.
[13] Foster P, Abdelal G, Murphy A. Quantifying the influence of lightning strike pressure loading on composite specimen damage. Appl Compos Mater 2018;26:115–37. https://doi.org/10.1007/s10443-018-9685-1.
[14] Li Y, Sun J, Li S, Tian X, Yao X, Wang B, et al. An experimental study of impulse-current-induced mechanical effects on laminated carbon fibre-reinforced polymer composites. Compos B Eng 2021;225:109245. https://doi.org/10.1016/j.compositesb.2021.109245.
[15] Sun J, Li Y, Tian X, Duan Y, Yao X, Wang B. Experimental and numerical analysis of damage mechanisms for carbon fiber-reinforced polymer composites subjected to lightning strikes. Eng Fail Anal 2020;118. https://doi.org/10.1016/j.engfailanal.2020.104894.
[16] Millen SLJ, Murphy A, Catalanotti G, Abdelal G. Coupled thermal-mechanical progressive damage model with strain and heating rate effects for lightning strike damage assessment. Appl Compos Mater 2019;26:1437–59. https://doi.org/10.1007/s10443-019-09789-z.
[17] Foster P, Abdelal G, Murphy A. Modelling of mechanical failure due to constrained thermal expansion at the lightning arc attachment point in carbon fibre epoxy composite material. Eng Fail Anal 2018;94:364–78. https://doi.org/10.1016/j.engfailanal.2018.08.003.
[18] Millen SLJ, Murphy A, Abdelal G, Catalanotti G. Sequential finite element modelling of lightning arc plasma and composite specimen thermal-electric damage. Comput Struct 2019;222:48–62. https://doi.org/10.1016/j.compstruc.2019.06.005.
[19] Wang FS, Yu XS, Jia SQ, Li P. Experimental and numerical study on residual strength of aircraft carbon/epoxy composite after lightning strike. Aerosp Sci Technol 2018;75:304–14. https://doi.org/10.1016/j.ast.2018.01.029.
[20] Wang FS, Ding N, Liu ZQ, Ji YY, Yue ZF. Ablation damage characteristic and residual strength prediction of carbon fiber/epoxy composite suffered from lightning strike. Compos Struct 2014;117:222–33. https://doi.org/10.1016/j.compstruct.2014.06.029.
[21] Harrell TM, Thomsen OT, Dulieu-Barton JM. Predicting the effect of lightning strike damage on the structural response of CFRP wind blade sparcap laminates. Compos Struct 2023;116707. https://doi.org/10.1016/j.compstruct.2023.116707.
[22] McQuien JS, Hoos KH, Ferguson LA, Iarve EV, Mollenhauer DH. Geometrically nonlinear regularized extended finite element analysis of compression after impact in composite laminates. Compos A Appl Sci Manuf 2020;134. https://doi.org/10.1016/j.compositesa.2020.105907.
[23] Falcó O, Lopes CS, Sommer DE, Thomson D, Ávila RL, Tijs BHAH. Experimental analysis and simulation of low-velocity impact damage of composite laminates. Compos Struct 2022;287:115278. https://doi.org/10.1016/j.compstruct.2022.115278.
[24] Sun XC, Hallett SR. Failure mechanisms and damage evolution of laminated composites under compression after impact (CAI): experimental and numerical study. Compos A Appl Sci Manuf 2018;104:41–59. https://doi.org/10.1016/j.compositesa.2017.10.026.
[25] Soto A, González EV, Maimí P, Martín de la Escalera F, Sainz de Aja JR, Alvarez E. Low velocity impact and compression after impact simulation of thin ply laminates. Compos A Appl Sci Manuf 2018;109:413–27. https://doi.org/10.1016/j.compositesa.2018.03.017.
[26] Lyu Q, Wang B, Guo Z. Predicting post-impact compression strength of composite laminates under multiple low-velocity impacts. Compos A Appl Sci Manuf 2023;164. https://doi.org/10.1016/j.compositesa.2022.107322.
[27] Xia Q, Zhang Z, Mei H, Liu Y, Leng J. A double-layered composite for lightning strike protection via conductive and thermal protection. Compos Commun 2020;21. https://doi.org/10.1016/j.coco.2020.100403.
[28] Feraboli P, Miller M. Damage resistance and tolerance of carbon/epoxy composite coupons subjected to simulated lightning strike. Compos A Appl Sci Manuf 2009;40:954–67. https://doi.org/10.1016/j.compositesa.2009.04.025.
[29] Kumar V, Yokozeki T, Okada T, Hirano Y, Goto T, Takahashi T, et al. Polyaniline-based all-polymeric adhesive layer: An effective lightning strike protection technology for high residual mechanical strength of CFRPs. Compos Sci Technol 2019;172:49–57. https://doi.org/10.1016/j.compscitech.2019.01.006.
[30] Guo Y, Xu Y, Zhang L, Wei X, Dong Q, Yi X, et al. Implementation of fiberglass in carbon fiber composites as an isolation layer that enhances lightning strike protection. Compos Sci Technol 2019;174:117–24. https://doi.org/10.1016/j.compscitech.2019.02.023.
[31] Kumar V, Yeole PS, Hiremath N, Spencer R, Masum Billah KM, Vaidya U, et al. Internal arcing and lightning strike damage in short carbon fiber reinforced thermoplastic composites. Compos Sci Technol 2020:112490. https://doi.org/10.1016/j.compscitech.2020.108525.
[32] Wang B, Ming Y, Zhu Y, Yao X, Ziegmann G, Xiao H, et al. Fabrication of continuous carbon fiber mesh for lightning protection of large-scale wind-turbine blade by electron beam cured printing. Addit Manuf 2020;31:100967. https://doi.org/10.1016/j.addma.2019.100967.
[33] Yamashita S, Hirano Y, Sonehara T, Takahashi J, Kawabe K, Murakami T. Residual mechanical properties of carbon fibre reinforced thermoplastics with thin-ply prepreg after simulated lightning strike. Compos A Appl Sci Manuf 2017;101:185–94. https://doi.org/10.1016/j.compositesa.2017.06.002.
[34] Hirano Y, Yokozeki T, Ishida Y, Goto T, Takahashi T, Qian D, et al. Lightning damage suppression in a carbon fiber-reinforced polymer with a polyaniline-based conductive thermoset matrix. Compos Sci Technol 2016;127:1–7. https://doi.org/10.1016/j.compscitech.2016.02.022.
[35] Xu X, Millen SLJ, Lee J, Abdelal GF, Mitchard D, Wisnom MR, et al. Developing test methods for compression after lightning strikes. Appl Compos Mater 2023. https://doi.org/10.1007/s10443-022-10100-w.
[36] Yin JJ, Li SL, Yao XL, Chang F, Li LK, Zhang XH. Lightning strike ablation damage characteristic analysis for carbon fiber/epoxy composite laminate with fastener. Appl Compos Mater 2016;23:821–37. https://doi.org/10.1007/s10443-016-9487-2.
[37] Foster P, Abdelal G, Murphy A. Understanding how arc attachment behaviour influences the prediction of composite specimen thermal loading during an artificial lightning strike test. Compos Struct 2018;192:671–83. https://doi.org/10.1016/j.compstruct.2018.03.039.
[38] Millen SLJ, Murphy A. Spatial and temporal Waveform A and B loading and material data for lightning strike simulations based on converged FE Meshes 2021. https://doi.org/10.17034/ef3ff864-78d3-4ce4-9c0f-fec7b4c408a0.

[39] Abdelal GF, Murphy A. Nonlinear numerical modelling of lightning strike effect on composite panels with temperature dependent material properties. Compos Struct 2014;109:268–78. https://doi.org/10.1016/j.compstruct.2013.11.007.
[40] Millen SLJ, Kumar V, Murphy A. The influence of carbon fiber composite specimen design parameters on artificial lightning strike current dissipation and material thermal damage. SAE Int J Aerosp 2023;16. https://doi.org/10.4271/01-16-02-0017.
[41] Sauder C, Lamon J, Pailler R. Thermomechanical properties of carbon fibres at high temperatures (up to 2000 °C). Compos Sci Technol 2002;62:499–504. https://doi.org/10.1016/S0266-3538(01)00140-3.
[42] Puck A, Schurmann H. Failure analysis of FRP lamninates by means of physically based phenomenological models. Compos Sci Technol 2002;62:1633–62. https://doi.org/10.1016/S0266-3538(96)00140-6.
[43] Tan W, Falzon BG, Chiu LNS, Price M. Predicting low velocity impact damage and Compression-After-Impact (CAI) behaviour of composite laminates. Compos A Appl Sci Manuf 2015;71:212–26. https://doi.org/10.1016/j.compositesa.2015.01.025.
[44] ABAQUS 2016 Documentation. ABAQUS Theory Manual. 2017.
[45] Lee J, Lacy TE, Pittman CU, Reddy JN. Numerical estimations of lightning-induced mechanical damage in carbon/epoxy composites using shock wave overpressure and equivalent air blast overpressure. Compos Struct 2019:224. https://doi.org/10.1016/j.compstruct.2019.111039.
[46] Benzeggagh ML, Kenane M. Measurement of mixed-mode delamination fracture toughness of unidirectional glass/epoxy composites with mixed-modebending apparatus 1996;56:1–11.
[47] Wisnom MR, Hallett SR, Soutis C. Scaling effects in notched composites. J Compos Mater 2010;44:195–210. https://doi.org/10.1177/0021998309339865.
[48] Millen SLJ, Lee J. Microscale modelling of lightning damage in fibre-reinforced composites. J Compos Mater 2023:57. https://doi.org/10.1177/00219983231163271.

2023-08-06

# Towards a virtual test framework to predict residual compressive strength after lightning strikes

Millen, Scott L. J.

Elsevier

Millen SLJ, Xu X, Lee J, et al., (2023) Towards a virtual test framework to predict residual compressive strength after lightning strikes. Composites Part A: Applied Science and Manufacturing, Volume 174, November 2023, Article number 107712

https://doi.org/10.1016/j.compositesa.2023.107712